

## Direct Simulation of the Time-Dependent Ginzburg-Landau Equation for Type-II Superconducting Thin Film: Vortex Dynamics and $V$ - $I$ Characteristics

Masahiko Machida\* and Hideo Kaburaki

*Computing and Information Systems Center, Japan Atomic Energy Research Institute,  
Tokai-mura, Naka-gun, Ibaraki 319-11, Japan*

(Received 26 July 1993)

We obtain the  $V$ - $I$  characteristics of the type-II superconductors for thin film by numerically solving the time-dependent Ginzburg-Landau equation coupled with the Maxwell equation in the two-dimensional region. We observe a sequence of pulses in the time development of the measured voltage, leading to intense energy dissipation in superconductors. We show that these voltage pulses are related to the penetration and annihilation of vortices at the boundary and the annihilation of two merging vortices with opposite sign.

PACS numbers: 74.60.Ge, 74.76.-w

In type-II superconductors, the dissipative mechanism of the superconducting current carrying state is mainly attributed to the magnetic quantized flux motion and its transport properties have been derived from flux dynamics. From the standpoint of the application of type-II superconductors, it becomes increasingly important to evaluate the  $V$ - $I$  characteristics and its relation to the vortex dissipation process. The basic dissipative mechanism by vortex motion has been explained by a simple classical electromagnetic dynamics model [1], the irreversible entropy flow model [2], and the time-dependent Ginzburg-Landau (TDGL) equation [3,4]. However, complex dynamics of these vortices is not well understood due to their strong nonlinear interactions.

Among these methods, the approach using the TDGL equation is effective in predicting the qualitative properties of vortex motions in type-II superconductors. Since the TDGL equation is nonlinear due to the higher order expansion terms of the order parameter, the theoretical approach is limited to a perturbative analysis based on the approximate form of the TDGL equation near the upper critical field  $H_{c2}$ . Therefore, the direct numerical simulation is the only way to treat rigorously the nonlinear dynamics of flux penetration process and interacting vortices.

Several numerical simulations using the full TDGL equation coupled with the Maxwell equation have been reported. Moriarty, Myers, and Rebbi studied the dynamical interactions of two colliding vortices [5]. Liu, Mondello, and Goldenfeld and Frahm, Ulah, and Dorsey studied the dynamics of the superconducting phase by changing the value of the Ginzburg-Landau (GL) parameter  $\kappa$  from the type-I to the type-II region [6,7]. Kato, Enomoto, and Maekawa studied the magnetization process [8] and presented the hysteresis curve of magnetization. However, there are almost no numerical studies on the transport properties and vortex dynamics in the presence of the constant external current and magnetic field except for the one-dimensional superconducting narrow filament [9].

Dissipation by vortex motions has been focused on in

the experiments using the narrow strip [10,11]. In a small sample like this, the averaged voltage and time fluctuating voltage component are dependent on the configurations and the number of vortices. For the study of these mesoscopic phenomena, computer simulation of the TDGL equation gives a clue to the complex nonlinear dynamics of vortices.

In this Letter, the direct simulation of the TDGL equation has been performed in the two-dimensional region and the dissipation process of superconducting current by vortex motions has been studied under the externally applied constant current and magnetic field. A sequence of pulses in the measured voltage [12,13] has been explained by the numerical results of time-dependent behavior of vortices using the perfect homogeneous superconductor.

In addition, the  $V$ - $I$  characteristics under the external magnetic field were obtained by averaging the time-dependent voltage.

We employ the macroscopic TDGL equation, which was derived by Gor'kov and Eliashberg from the microscopic theory [14]:

$$D^{-1} \left[ \frac{\partial}{\partial t} + i \frac{2e\varphi}{\hbar} \right] \Delta + \xi^{-2} (|\Delta|^2 - 1) \Delta + \left[ \frac{\nabla}{i} - \frac{2e}{\hbar c} \mathbf{A} \right]^2 \Delta = 0,$$

$$\mathbf{j} = \sigma \left[ -\nabla\varphi - \frac{1}{c} \frac{\partial \mathbf{A}}{\partial t} \right] + \text{Re} \left[ \Delta^* \left[ \frac{\nabla}{i} - \frac{2e}{\hbar c} \mathbf{A} \right] \Delta \right] \frac{\hbar c^2}{8\pi e \lambda^2}. \quad (1)$$

In these equations, the time  $t$ , coordinate vector  $\mathbf{r}$ , order parameter  $\Delta$ , and vector potential  $\mathbf{A}$  are rescaled using  $4\pi\sigma\xi(0)^2\kappa^2/c^2$ ,  $\xi(0)$ ,  $\Delta(0)$ , and  $H_{c2}(0)\xi(0)$ . Here,  $\varphi$  is the scalar potential,  $\xi$  is the coherence length,  $\lambda$  is the penetration depth, and Re means taking the real part. For simplicity we use the gauge fixing condition of  $\varphi = 0$ .

Equations (1) are discretized using the method employed in [5,7,8]. Here the link variable  $U_{ij} = \exp(i\mathbf{A}_{ij})$ , where  $ij$  represents a pair of nearest lattice sites, is used and the order parameter and the gauge field are defined on the lattice site and the link between the sites, respec-

tively [15]. With the introduction of this link variable, the discretized equations conserve the gauge invariant properties which are intrinsic in the continuous equations (1) [8].

The two-dimensional rectangular superconducting thin film sandwiched between the normal conductors (see Fig. 1) is employed as a computational region. Here, for simplicity, the diamagnetization effect for the applied field and the  $z$ -direction dependence of order parameter and vector potential are neglected. It is assumed that the constant external normal current homogeneously flows into the superconducting region from one side and flows out to the other normal conductor.

In the presence of the external applied current, a local magnetic field for the Maxwell equation and a gauge covariant first derivative of the order parameter for the TDGL equation are required for the boundary conditions. The local field in the upper and lower boundaries, parallel to the direction of the external current, is given by the sum of the current-induced magnetic field  $H_i$  and the applied magnetic field  $H_a$ . The current-induced magnetic field  $H_i$  is  $Wj_i/2$  for the upper boundary and  $-Wj_i/2$  for the lower boundary, where  $j_i$  is the external transport current density and  $W$  is the width of the superconducting region. This condition implies that the conservation of the total current on any line perpendicular to the transport current holds in the computational region. The local magnetic field on inlet and outlet boundaries is taken to be the sum of the applied magnetic field and the induced field by the uniform constant external normal current. In the case of the zero applied magnetic field, the current-induced magnetic field generates vortices with different signs. Therefore, vortices appear in the upper computational region, while antivortices appear in the lower part.

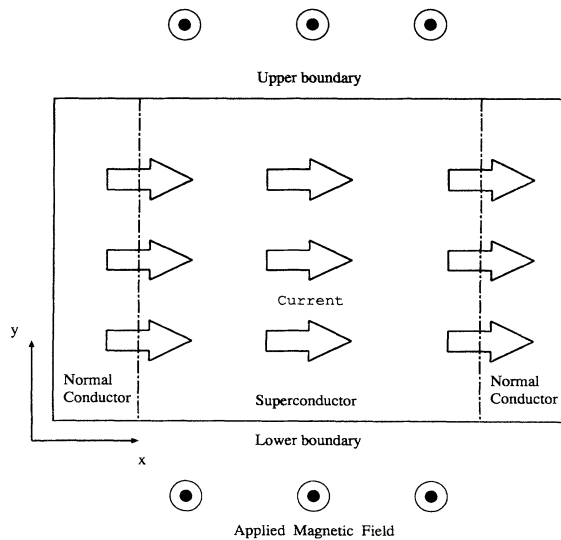


FIG. 1. The computational region in which the superconductor is sandwiched between the normal conductors. The upper and lower boundaries are exposed to a vacuum space.

The first derivatives of the order parameter in all boundaries are set to be zero. The initial conditions are that all order parameters  $\Delta$  are equilibrium values,  $\Delta(T) = \Delta(0)(1 - T/T_c)^{1/2}$ , and all link variables  $U_{ij}$  are unity corresponding to the zero applied field. In the present simulation, the GL parameter  $\kappa$  is assumed to be 2.0, the critical superconducting transition temperature  $T_c$  to be 20 K, the measuring temperature  $T$  to be 10 K, the time step to be 0.001, and the computational region to be  $40\xi(0) \times 40\xi(0)$ .

The external field is gradually applied during the first 140000 steps for the purpose of reaching the steady non-equilibrium state in a stable manner.

Here, we show the simulation results. First, for the case of the applied magnetic field of  $H_a = 0.2H_{c2}(10 \text{ K})$  and the external current of  $j_i = 0.034$ , Figs. 2(a)-2(c) show snapshots of the typical distribution of the order parameter, supercurrent, and normal current, respectively, in the steady flux flow region. The vortex penetration is found to be initiated at the magnetic field larger than the lower critical field  $H_{c1}(10 \text{ K})$ . This phenomenon was also reported in [8] on the magnetization process and was attributed to the surface barrier against vortex nucleation. From Fig. 2(c) it is seen that the normal current, which flows into the superconducting region at the inlet boundary, turns into a superconducting current and reappears at the outlet boundary. It is shown in Fig. 2(c) that the induced electric field for the normal current distribution, which is identified as the electric dipole moment field described by Bardeen and Stephen [1], appears where the supercurrent vortex exists. It becomes possible to evaluate the dissipation of superconducting current by studying the electric field generated by this vortex motion. Figure 3 is the voltage distribution  $V(x)$  as a function of the distance from the inlet of the applied current. This voltage is defined as the average of the  $x$  component of the local electric field  $\mathbf{e}$  in the  $y$  direction  $V(x) = V(0) + W^{-1}(\int_W \mathbf{e}_x dy)$ . It is found that except near the inlet and outlet boundaries the voltage gradient is nearly zero below the critical current, where vortices do not appear, while a finite gradient by vortex motion is observed above the critical current as shown in Fig. 3.

Figure 4 is the characteristic time development of the measured voltage in the presence of the applied magnetic field  $H_a = 0.2H_{c2}(10 \text{ K})$  and the external transport current  $j_i = 0.03$ . It is found that the voltage shows a sequence of periodic pulses. With the increase of the transport current, a pulse becomes more sharpened and the interval between pulses is reduced. If the current is further increased, a sequence of random overlapping pulses appears. In our numerical results, these voltage pulses are found to be related to vortex motions. It is observed that a pulse of voltage with a sharp peak is generated when a vortex is created or annihilated at the upper and lower boundaries. These phenomena are caused by the intense surface current which gives rise to the effective strong force on vortices near the boundaries. The interval be-

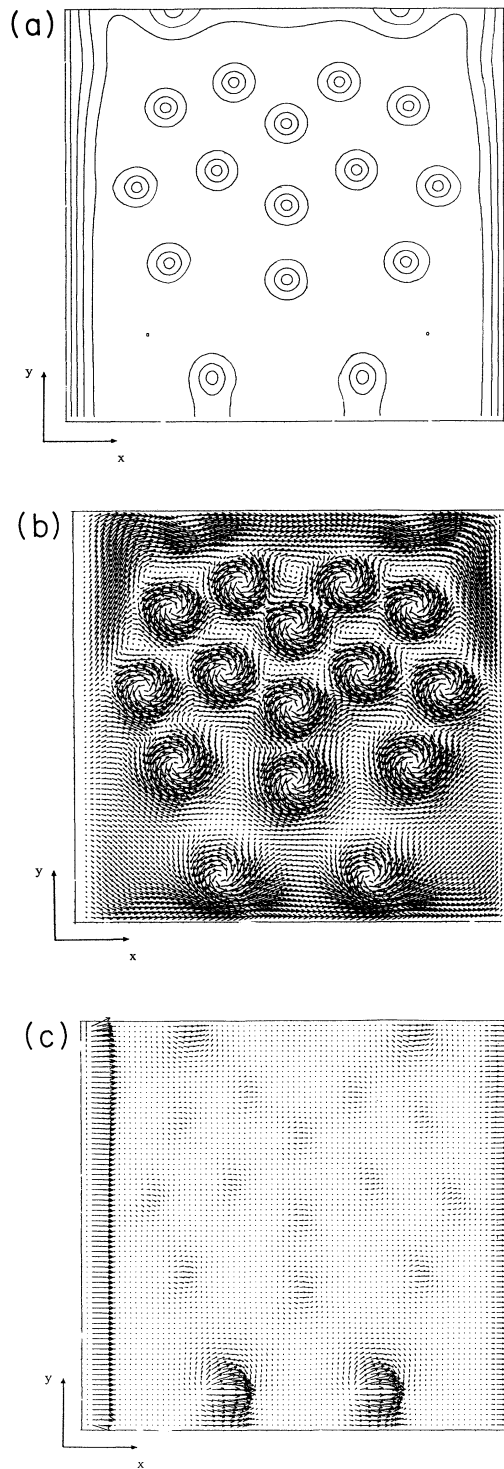


FIG. 2. (a) Snapshot of the spatial distribution of the order parameter for  $T=10$  K ( $T_c=20$  K),  $H_a=0.3H_{c2}$  (10 K),  $j_i=0.034$ , and 400000 steps. (b) Snapshot of the spatial distribution of the supercurrent. The numerical condition is the same as that in (a). (c) Snapshot of the spatial distribution of the normal current. The numerical condition is the same as that in (a).

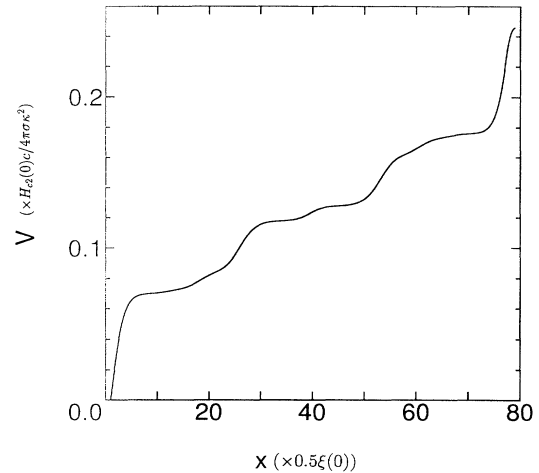


FIG. 3. Snapshot of the measured voltage as a function of the  $x$  direction. The numerical condition is the same as that in Fig. 2(a).

tween pulses is explained by the convection of vortices over the computational region. When the applied magnetic field is zero or very weak, it is found that there is another intense dissipative mechanism, in which the vortex and antivortex, generated by the current-induced magnetic field, merge around the center of the computational region. It is also found that the attractive interaction between vortices and antivortices enhances the speed of the vortex motion and thus increases the dissipation.

Figures 5(a) and 5(b) are the distributions for the super and normal current, respectively, when two vortices with opposite signs interact. Figure 5(a) shows the instant when two vortex pairs and an isolated vortex interact strongly, while Fig. 5(b) indicates the existence of the strong dissipation in merging vortex pairs.

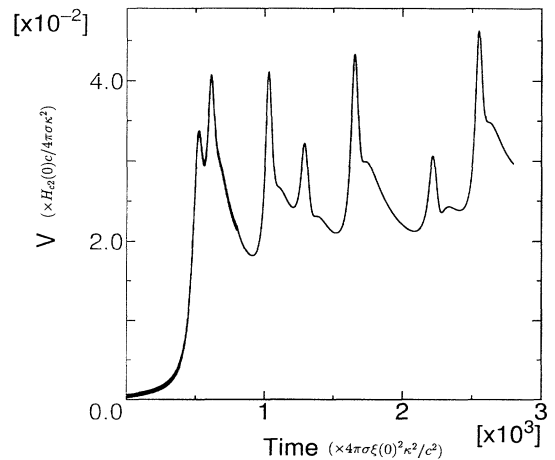


FIG. 4. The time development of the measured voltage for  $T=10$  K ( $T_c=20$  K),  $H_a=0.2H_{c2}$  (10 K), and  $j_i=0.03$ .

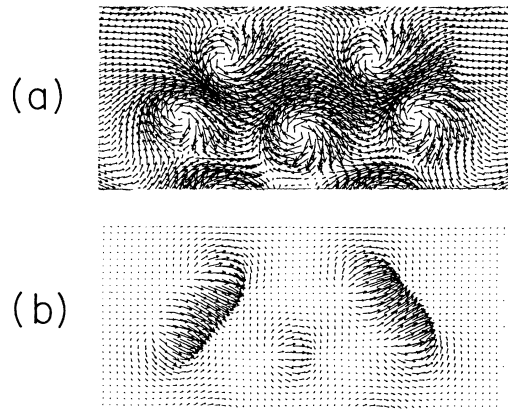


FIG. 5. (a) The supercurrent distribution in which a vortex and an antivortex interact. (b) The normal current distribution which corresponds to (a).

The voltage-current ( $V$ - $I$ ) characteristics in the present simulation have been shown in Fig. 6. Here, the steep voltage gradient near the inlet and outlet boundaries, which is seen in Fig. 3, is neglected and only the internal voltage gradient in the steady state of vortex motions is calculated. The voltage is averaged for computational time steps of 360000. This averaged time is sufficiently long for a single vortex to move from one region boundary to the other. In Fig. 6, the case of  $H_a=0$  shows the  $V$ - $I$  characteristics for the flux flow generated only by the current-induced field. It is found that the abrupt increase of voltage, followed by an initial slow increase, is caused by the formation of the train of vortices across the direction of the external current where a normal conducting domain prevails in this region. This phenomenon is well known for the experiments using a narrow strip of the type-I superconductor. Here, even in type-II superconductors, it is shown that the growth of the extended normal domain is observed in the high current region. It is seen in Fig. 6 that the voltage-current relation becomes linear as the external magnetic field is increased,  $H=0.2, 0.4, 0.6H_{c2}(10\text{ K})$ . For the slowly increasing region in the voltage-current characteristics, a few vortices are observed. On the other hand, a large number of vortices dominate the superconducting region and the steady flux flow appears in the linearly increasing region.

In conclusion, we have developed the numerical technique using the TDGL and the Maxwell equations in the presence of the external current and magnetic field. Using the two-dimensional geometry, we have succeeded in the simulation of the vortex nucleation and flux flow, and the evaluation of the  $V$ - $I$  characteristics. In addition, the dynamical properties such as time-dependent voltage are derived and its intense dissipative mechanisms related to vortex motions are clarified. We believe that a recent improved mesoscopic experimental measurement will be

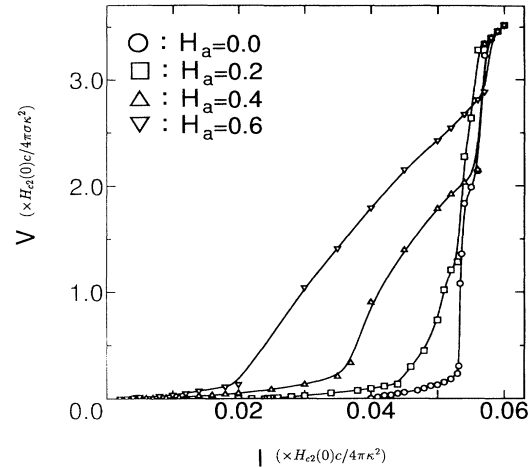


FIG. 6. The  $V$ - $I$  characteristics for different external magnetic fields [ $H_a=0.0, 0.2, 0.4, \text{ and } 0.6H_{c2}(10\text{ K})$ ].

able to confirm the present results.

One of the authors (M.M.) is indebted to Professor M. Tachiki, Professor H. Matsumoto, Dr. T. Koyama, and Dr. S. Takahashi of the Institute for Materials Research, Tohoku University for valuable discussions and comments.

\*On leave from Fujitsu Ltd., R&D Systems Department, 1-9-3 Nakase, Mihama-ku, Chiba-shi 261, Japan.

- [1] J. Bardeen and M. J. Stephen, Phys. Rev. **140**, 197 (1965).
- [2] J. R. Clem, Phys. Rev. Lett. **20**, 735 (1968).
- [3] K. Maki, Phys. Rev. **169**, 381 (1968).
- [4] C. R. Hu and R. S. Thompson, Phys. Rev. B **6**, 110 (1972).
- [5] K. J. M. Moriarty, E. Myers, and C. Rebbi, Phys. Lett. B **207**, 411 (1988).
- [6] F. Liu, M. Mondello, and N. Goldenfeld, Phys. Rev. Lett. **66**, 3071 (1991).
- [7] H. Frahm, S. Ulah, and A. T. Dorsey, Phys. Rev. Lett. **66**, 3067 (1991).
- [8] R. Kato, Y. Enomoto, and S. Maekawa, Phys. Rev. B **47**, 8016 (1993).
- [9] R. J. Watts-Tobin, Y. Kráhenbühl, and L. Kramer, J. Low. Temp. Phys. **42**, 459 (1981).
- [10] Y. Ando, H. Kubota, and S. Tanaka, Phys. Rev. Lett. **69**, 2851 (1992).
- [11] Y. Ando, H. Kubota, S. Tanaka, M. Aoyagi, H. Akoh, and S. Takada, Phys. Rev. B **47**, 5481 (1993).
- [12] J. R. Clem, Phys. Rep. **75**, 1 (1981).
- [13] B. Placais, P. Mathieu, and Y. Simon, Phys. Rev. Lett. **70**, 1521 (1993).
- [14] L. P. Gor'kov and G. M. Eliashberg, Zh. Eksp. Teor. Fiz. **54**, 612 (1968) [Sov. Phys. JETP **27**, 328 (1968)].
- [15] J. B. Kogut, Rev. Mod. Phys. **51**, 659 (1979).